DOI: 10.1002/smll.200500479

Electrospray Ion Beam Deposition of Clusters and Biomolecules

Stephan Rauschenbach, Frank L. Stadler, Eugenio Lunedei, Nicola Malinowski, Sergej Koltsov, Giovanni Costantini, and Klaus Kern*

An ion beam source using electrospray ionization is presented for non-destructive vacuum deposition of mass-selected large organic molecules and inorganic clusters. Electrospray ionization is used to create an ion beam from a solution containing the nanoparticles or molecules to be deposited. To form and guide the ion beam, radio frequency and electrostatic ion optics are utilized. The kinetic energy distribution of the particles is measured to control the beam formation and the landing process. The particle mass-to-charge ratio is analyzed by in situ time-of-flight mass spectrometry. To demonstrate the performance of the setup, deposition experiments with gold nanoclusters and bovine serum albumin proteins on graphite surfaces were performed and analyzed by ex situ atomic force microscopy. The small gold clusters are found to form three-dimensional agglomerations at the surface, preferentially decorating the step edges. In contrast, bovine serum albumin creates two-dimensional fractal nanostructures on the substrate terraces due to strong intermolecular interactions.

Keywords:
- biomolecules
- clusters
- electrospray ionization
- epitaxy
- mass spectrometry

1. Introduction

The surface deposition of organic molecules recently became an important topic due to technological developments in biotechnology, organic electronics, and functional materials. Research in the field of proteomics[1] and the development of organic light-emitting diodes (OLEDs)[2] are good examples of the wide-ranging applications of organic molecules at surfaces. OLEDs are manufactured within the limitations of semiconductor technology implying that the production environment needs to be very clean and controlled. In order to achieve proper device performance, impurity concentrations have to be in the order of 10^{10} cm^{-3}.[3] Therefore the growth of the organic materials needs to take place in vacuum, where at present only small molecules can be deposited by means of organic molecular beam epitaxy (OMBE). Larger molecules typically exhibit lower vapor pressures and are unstable at elevated temperatures, with the consequence that they decompose before sublimation. The very same limitation concerns research on biological molecules, where no general vacuum deposition technique can be applied. In contrast, the study of fundamental interactions of biomolecules with surfaces and with each other would greatly profit from a precisely controlled environment and from atomic-scale analytical techniques, both available only in ultrahigh vacuum.[4] Furthermore, the functionalization of surfaces with organic and biological molecules is of fundamental importance in molecular nanotechnology, opening many new opportunities ranging from mo-

[*] S. Rauschenbach, Dr. F. L. Stadler, Dr. E. Lunedei, Dr. N. Malinowski, Dr. G. Costantini, Prof. K. Kern
Max-Planck-Institute for Solid State Research
Nanoscale Science Department, Heisenbergstr. 1
70569 Stuttgart (Germany)
Fax: (+49) 711-689-1662
E-mail: s.rauschenbach@fkf.mpg.de
Dr. S. Koltsov
Institute for Analytical Instrumentation
Russian Academy of Science, 18813 St. Petersburg (Russia)

NANO MICRO small

lecular electronics[5] to specific biological recognition and sensor applications.[6]

The electrospray ionization (ESI) technique was originally developed to overcome the problem of destruction-free creation of charged-particle beams for mass spectrometry applications.[7] By ionizing droplets of a solution containing the analyte molecules and later drying off the solvent, electrospray ionization is capable of creating an ion beam of molecules that otherwise could not be transferred into the gas phase. A wide range of applicability was demonstrated in the field of mass spectrometry as well as for sample preparation purposes. For example, viruses with masses up to 4×10^7 Da were analyzed by electrospray mass spectrometry, surface deposited, and then found in their native structure, still being infective.[8] Besides a vast number of organic substances, proteins have also been investigated and proven to have kept their biological activity after being deposited from an electrospray ion source.[9] Moreover, deposition experiments were carried out using many other materials such as polymers, transuranium ions, or semiconductor clusters.[10]

Destruction-free ionization is not the only requirement for deposition experiments. In addition, a gentle deposition technique is needed in order to bring the molecules intact to the surface. For the case of nanoscale metallic clusters, kinetic energies lower than approximately 1 eV per atom ensure a soft landing.[11] For organic molecules, as well as for proteins, soft landing conditions have been defined as those preserving a specific type of functionality. This has been achieved for energies of about 1 eV per charge, although the precise value depends on the particular type of molecule and on its interaction with the substrate surface.[12] For enzymes, a kinetic energy of 3 eV per charge was found to be an optimal deposition energy, while at 10 eV per charge the enzyme activity dropped severely after deposition. This indicates that some process during collision with the substrate altered the enzyme properties. The energy limits for the soft deposition of smaller organic ions may be as high as 5 eV per charge.[13]

In order to perform deposition experiments with large organic and biological molecules, as well as with inorganic clusters, a multipurpose ion beam source was designed and built. Here we present an experimental setup that combines several techniques: electrospray ionization as a beam source, differential pumping to overcome the gap between atmospheric pressure and high vacuum, ion optics to guide the beam, a time-of-flight (TOF) mass spectrometer to monitor the beam composition, and a gentle vacuum deposition. With this apparatus we were able to create a stable beam from several kinds of nanoparticles for their controlled deposition. Extremely diluted thin films were prepared on solid substrates and characterized by atomic force microscopy.

2. Results and Discussion

In an initial series of experiments the fundamental properties of the beam were analyzed using a movable Faraday cup. A solution of rhodamine 6G (Aldrich, $M_w = 479$ Da) was used without further treatment. The solution contained 1 mg rhodamine in a 10 mL mixture of water and ethanol (1:1). In order to reach a higher current, the solution was made acidic (pH 3–4) by adding acetic acid. To achieve a high beam current, the typically used radio-frequency (rf) voltage of 380 V at Q2 (see Figure 1 for the experimental

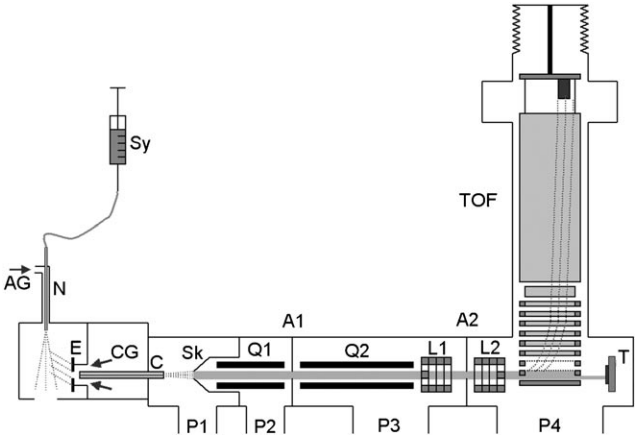

Figure 1. Scheme of the electrospray deposition source. The full length of the assembly is about 1 m. Sy: syringe with solution, N: spray needle, AG: assisting gas for the spray process, E: entrance plate counter electrode (−4 kV), CG: nitrogen counter gas, C: heated capillary, S: skimmer between first and second pumping stage, Q1: high-pressure quadrupole ion guide, A1: aperture between first and second ion guide, Q2: low-pressure quadrupole ion guide, L1, L2: lens system (einzel lens and steering plates), A2: aperture between third pumping stage and deposition chamber, TOF: movable orthogonal extraction time-of-flight mass spectrometer, T: deposition target. Pumping stages, P1: 1 mbar, P2: 0.1 mbar, P3: 10^{-4} mbar, P4: 10^{-6} mbar.

setup) was decreased to 340 V because the rhodamine molecule, although only singly charged,[14] is otherwise too light to be transmitted, as indicated in Figure 2. The beam energy was measured by sweeping the voltage of the electrostatic lens L2 located just in front of the detector and measuring the net current on the Faraday cup. The first derivative of the measured current–voltage characteristics (Figure 3a) represents the beam energy distribution. Its full width at half maximum represents the energy spread and its center the average beam energy per charge (Figure 3b).

The energy distribution of the beam was found to depend mainly on parameters connected to the first, high-pressure quadrupole ion guide. Raising the pressure in this pumping stage increases the number of collision events between the ions and the background gas. As a result the center of the energy distribution (related to the beam axial velocity) and the distribution width (connected with the beam spread) both drop (Figure 3c). The voltage applied to the aperture (A1) between the two quadrupoles also has an influence on the particle energy. When this quadrupole extraction voltage is increased, the energy distribution measured at the detector in the fourth chamber changes accordingly (Figure 3d).

By acting on these parameters for different spray solutions it was possible to tune the beam energy in the range between 5 eV and 50 eV per charge with a corresponding

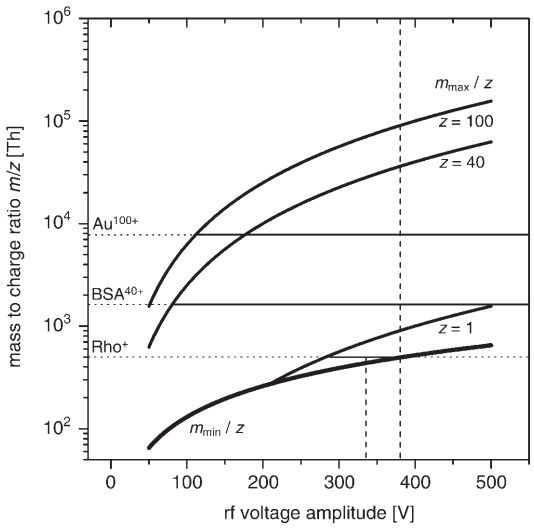

Figure 2. Minimum (m_{min}/z) and maximum (m_{max}/z) transmitted mass-to-charge-ratio (given in Thomson units; 1 Th = 1 amu per charge) for the quadrupole Q2 with an ion energy of 10 eV per charge. The mass-to-charge-values of the molecules used in the actual experiments are shown (Au^{100+}: gold colloids, BSA^{40+}: albumin, Rho^{+}: rhodamine) and the used voltages of 340 V for rhodamine and 380 V for albumin and the gold colloids are displayed.

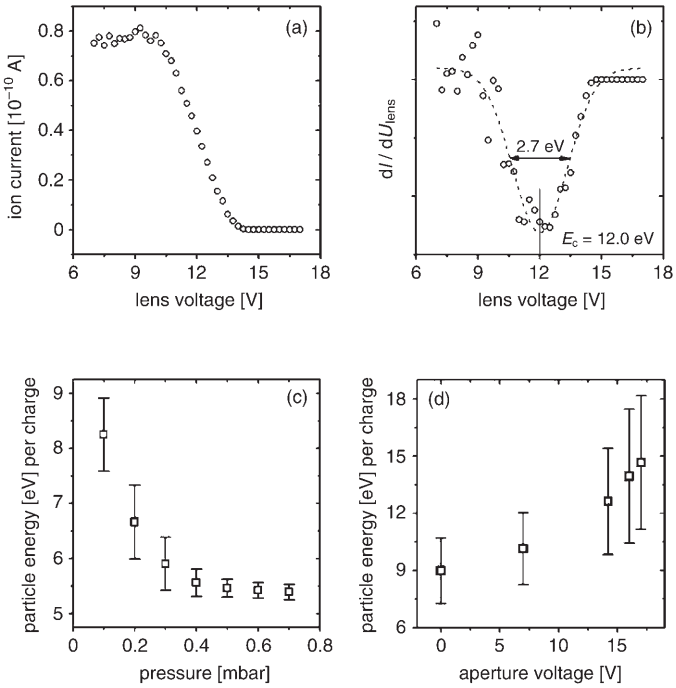

Figure 3. Beam characterization by means of a movable detector in the TOF chamber (10^{-6} mbar) and the lens L2. A lens voltage sweep creates a typical current signal (a) on the movable detector. The derivative of this signal represents the energy distribution of the beam (b). The pressure in the second pumping stage (c) and the voltage applied to the aperture A1 (d) can be used to adjust the mean beam energy (open squares) and the beam energy spread (error bars).

energy spread adjusted between 1 eV and 10 eV per charge. At the low range of this energy window, soft landing of rhodamine ions should be possible. The value of 5 eV per charge corresponds to energies for which soft landing of similar-sized organic ions was shown to be successful.[13] The kinetic energy of the heavier ions generated with the presented setup was found in the same order of magnitude. In order to achieve lower- or higher-incidence energies, a voltage can be applied to the sample. The available kinetic energy range then expends to between 0.5 and 70 eV. Since it can be controlled independently from the beam flux, the tunablility of the beam energy and its distribution is a key advantage of the electrospray ion source compared with OMBE. For the deposition experiments, organically functionalized gold clusters in a colloidal dispersion (Sigma G-1402, $\approx 8 \times 10^5$ Da) and bovine serum albumin (BSA, Sigma, 66300 Da) were used. Both gold and BSA were deposited on highly oriented pyrolytic graphite (HOPG) in the fourth pumping stage at 10^{-6} mbar and at room temperature.

The aqueous colloid dispersion contained 0.01% $HAuCl_4$, 0.01% tannic acid, 0.04% trisodium citrate, 0.26 mM KCO_3, and 0.02% sodium azide (Sigma) and the gold particles, which were nominally sized between 3.5 and 6.5 nm in diameter. A stable ion current of 5 pA was obtained for an incidence energy of 10 eV per charge by optimizing the source parameters. As, to the best of our knowledge, there is no comparable experiment reported, the charge of the colloids can only be estimated from the sample coverage and the deposition current. By doing so, a value of $\approx$100 elementary charges was calculated, thus resulting in a mass-to-charge-ratio of about 10^4 amu per charge. Even for this high mass-to-charge ratio, the transmission of the gold ions in Q2 is possible, as indicated in Figure 2. After deposition for 150 min, the samples were analyzed using tapping-mode atomic force microscopy (AFM) under ambient conditions.

Gold aggregations with diameters between 250 and 640 nm in diameter and 3 and 17 nm in height were found on the HOPG surface, preferentially at the step edges (Figure 4). The cluster size and density indicates that these agglomerations of gold colloids are formed on the surface. As a consequence, gold colloids have to be highly mobile on the surface as further testified by the step-edge decoration.

Uncoated gold clusters were found to rapidly diffuse on atomically clean HOPG substrates, where they form dendritically ramified islands.[15] Our experiments, in contrast, were performed with organically coated gold clusters, which can display significantly altered cluster surfaces as well as cluster–cluster interactions. The observed isolated three-dimensional structures indicate that the cluster agglomerations follow a Volmer–Weber growth mode, which implies a stronger interaction between the deposited particles than between the particles and the substrate.

Experiments with uncoated small metal cluster ions have been reported in the literature for deposition energies of 3 eV to 14 eV, which result in the formation of surface impact defects that act as pinning centers for cluster diffusion.[11] In our case, no evidence for pinning sites could be found. This was indicated by the diffusion of the gold colloids to the step edges. In the aforementioned experiments, the generation of pinning sites could be avoided by the dep-

NANO MICRO small

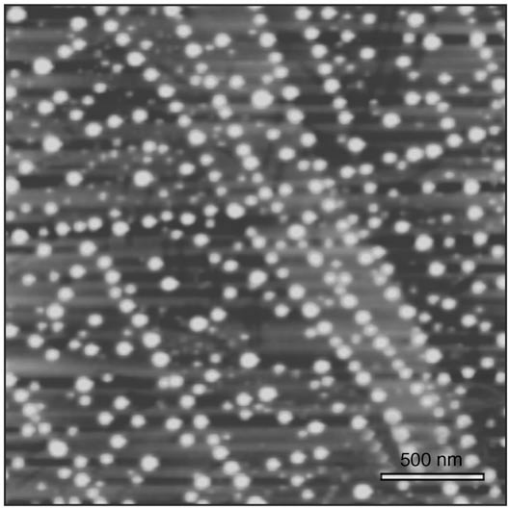

Figure 4. AFM topography of gold nanoparticles deposited in vacuum (10^{-6} mbar) on HOPG at room temperature. A current of 5 pA was used for 150 min. Large clusters with a height of 3–17 nm and a corresponding width of 250–640 nm decorate the step edges in particular.

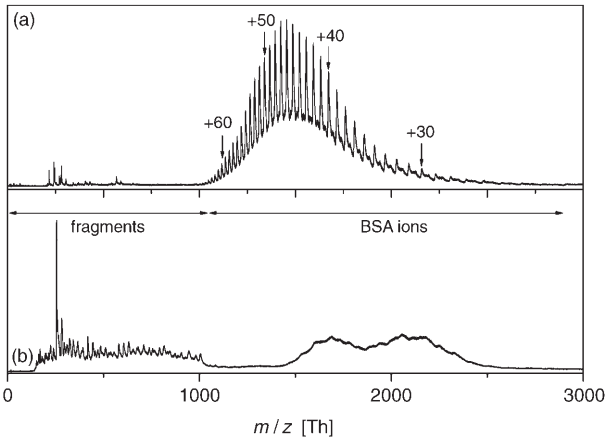

Figure 5. ESI-TOF mass spectra of bovine serum albumin (BSA)-sprayed from an acidic solution (0.1 mg mL^{-1} BSA in EtOH/H_2O (1:1) with 1% acidic acid) for two different fragmenting electrode voltages. a) For a fragmenting voltage of 100 V, the ion beam consists mainly of BSA molecules with a charge of $+65$ to $+25$. b) In the case of higher fragmenting voltages ($V_{frag}=180$–320 V), more fragments can be observed in the ion beam. Small fragments appear in the regioon up to 1000 Da, while the larger BSA fragments have similar mass-to-charge-ratios as the intact BSA ions. The larger BSA fragments actually appear in both spectra (a) and (b) as a broad background between 1000 Th and 2500 Th.

osition of a 10 nm argon buffer layer on the substrate at 10 K. This buffer layer absorbs the collision damage, while the cluster and the surface remain mainly unaffected. A similar role could have been played by the organic coating of the gold colloid ions that were deposited in our experiments with an energy of 10 eV per charge ($E \approx 1$ keV for 100 charges).

BSA was dissolved at a concentration of 1.5 μM in a H_2O:EtOH mixture (1:1). This solution was then made acidic by adding 1 vol% of acetic acid. Depending on the pH value, albumin sprayed from such solutions is known to have around 40 charges per molecule.[16] This corresponds to a mass-to-charge-ratio of about 1500 amu per charge, which is expected to be transmitted for a wide range of rf voltage, as indicated in Figure 2. ESI-TOF mass spectrometry demonstrates this result, when the Q2 quadrupole is used in a rf-only mode (see Figure 5a). Besides albumin ions with charges between $+70$ ($\approx$1000 Da) and $+25$ ($\approx$2500 Da), some fragment ions in the region up to 1000 Da were observed. In this configuration stable beams with currents of 20–40 pA were achieved for deposition. The deposition charge for sub-monolayer coverage was typically 10–50 pA h^{-1}. After deposition, the samples were analyzed by AFM (Figure 6).

Similar to the gold islands, the BSA molecules also show a step-edge decoration on HOPG. Furthermore, two-dimensional fractal clusters formed from BSA molecules are observed. These aggregates are not only formed at step edges but also on terraces. This indicates that BSA is less mobile on graphite than the gold clusters due to stronger molecule–surface interactions. The images for two different coverages (Figure 6 a,b for low coverage; c,d for high coverage) show fractal agglomerations. Even though the single building units (Figure 6b and d) of these islands appear nonuniform, their size is compatible with that of a single BSA molecule in aqueous solution (116 Å × 27 Å).[17]

To address the question of whether the BSA deposition can be considered as a soft landing process, further experiments were performed. In particular, deposition experiments were carried out as a function of the beam energy in the 0.5–65 eV range and with an intentionally created fragmented beam. Beams at different ion energies were prepared under conditions identical to those shown in Figure 5a. At the highest energies, deposition currents as high as 60 pA were measured due to better collimation. The fragmented beam was prepared by applying 350 V to the fragmenting electrode (Figure 5b) and by mass-selecting the resulting beam in Q2. Only the ions between 0 and 1000 Da, which correspond to BSA fragments, were allowed to pass the quadrupole. Due to the mass selection, the current at the sample was reduced to 8 pA and accordingly longer deposition times (up to 3 h) were employed.

The results obtained for intact ion beams with energies lower than 15 eV are identical to those shown in Figure 6. The situation is different for the high-energy ions (65 eV) and the fragmented ions. The corresponding surface morphologies are depicted in Figure 7a and b, respectively. At first sight, these AFM images also show the same fractal agglomerations seen in Figure 6; the only evident difference being the additional structures with diameters up to 100 nm in Figure 7b. Nevertheless, a detailed quantitative analysis shows that the fractal islands in Figure 7 actually differ in height from the soft-landed BSA proteins. The building units of the structures shown in Figure 6a–d have a height of 1.8 ± 0.3 nm, while those obtained from the fragment beam are only 0.8 ± 0.1 nm in height (Figure 7a). This smaller size is clearly due to the reduced mass of the fragments in respect to the intact BSA proteins (see Figure 5a). As a consequence, the height of 1.2 ± 0.3 nm measured for the

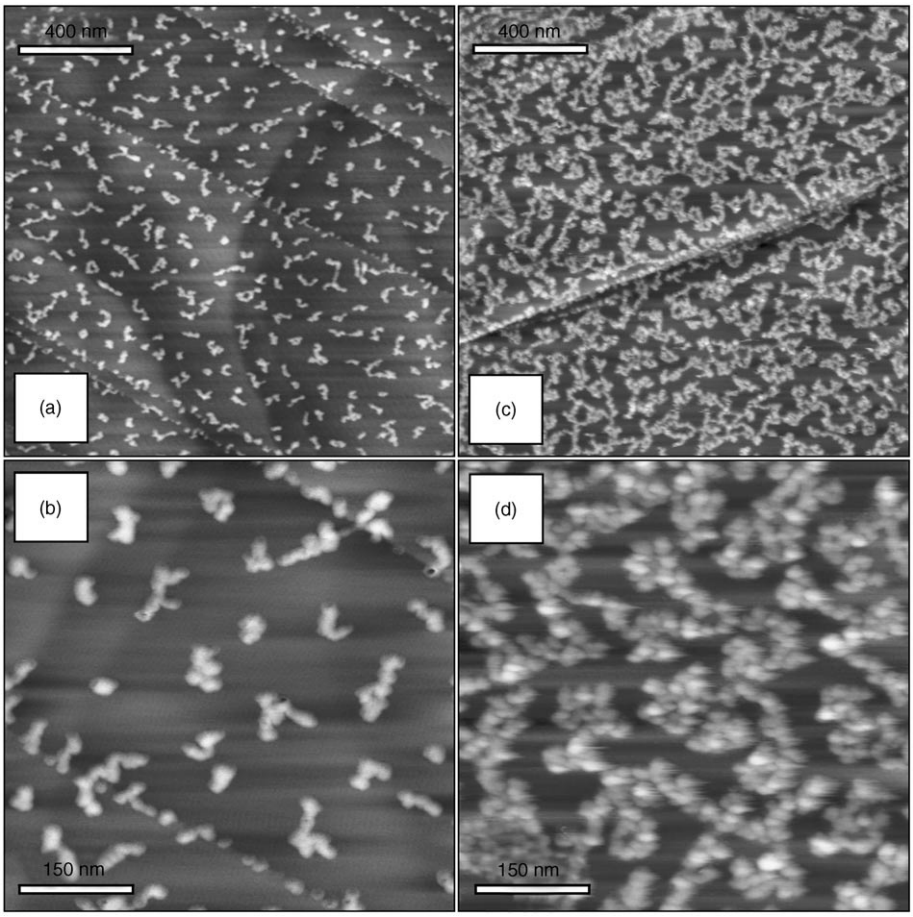

Figure 6. AFM topography of BSA deposited on HOPG under vacuum (10^{-6} mbar) at room temperature. An ion current of 30 pA was used for 85 min. Fractal aggregations formed by stringlike particles are found on the surface, indicating diffusion-limited aggregation. The spatial gradient of the beam intensity results in low (a, b) and high coverage (c, d) regions, which are close to the sample border and center, respectively.

structures formed by depositing 65 eV ions (Figure 7b) is an indication that energetic particle–surface collisions induce partial fragmentation of BSA.[13] Our observation that no fragmentation occurs at lower deposition energies agrees well with similar results reported in the literature.[12a]

The fact that a common fractal growth mechanism is observed for deposition experiments that produce building units of different sizes (low energy, high energy, and fragmented beam) implies that the particle–particle and the particle–substrate interactions are weakly dependent on the particle size. This could happen if the BSA proteins and their fragments are denaturated and assume a random coil conformation. As a matter of fact, proteins taken from their natural environment will in most cases change their structure. BSA is known to undergo structural changes in solution as a function of the pH value. In particular for low pH values, as are used for the spray solution in the present experiments, BSA unfolds partially to yield a stringlike molecule with four bulky centers along the string.[18] Further environmental stress can cause an even stronger unfolding and the protein then arranges into a random coil. The high-charged state of the BSA molecules observed with ESI-TOF mass spectrometry (Figure 5) indicates that the ion beam consists of unfolded or random coil protein ions.[19]

Since it is not very likely for a protein in the presence of an inorganic surface to fold back to its native structure (and it is obviously impossible for a fragment), it is reasonable to expect that both fractions and intact BSA molecules are present on the surface as random coils. This assumption accords very well with the observation that, independently of their size, the building units (shown in Figures 6 and 7) always appear nonuniform.

Because of the random coil structure, more and stronger reactive parts of the protein are made accessible, causing a substantial interaction with other molecules and with the substrate surface. This interaction is not strong enough to prevent the monomer from being mobile to some extent, but it, at least, inhibits the motion of bigger agglomerations. These nucleation conditions are very similar to those defining diffusion-limited-aggregation growth.[20] In fact, the fractal shape of the BSA clusters appears to be similar to aggregates formed under these conditions in various surface-supported atomic and molecular systems.[21]

3. Conclusions

We have presented an electrospray-based deposition source and shown its ability to overcome the limitations of vapor deposition for large molecules or clusters. The electrospray technique was used to create molecular as well as cluster ion beams. The composition of the beam can be analyzed in situ by time-of-flight mass spectrometry. Vacuum deposition was realized by a differential pumping system equipped with electrostatic and rf ion optics to guide the beam through four vacuum stages. Particle energies of 0.5 to 65 eV per charge were measured, allowing nondestructive landing for the lower end of this range even for heavily charged ions. The deposition was demonstrated with gold colloids and BSA proteins. Both molecules were found to preferentially decorate the step edges of the HOPG substrates, hence being mobile on the surface. The gold clusters exhibited three-dimensional island growth, caused by diffusion on the substrate surface. BSA was found to assemble into two-dimensional fractal aggregates. The observed struc-

NANO MICRO small

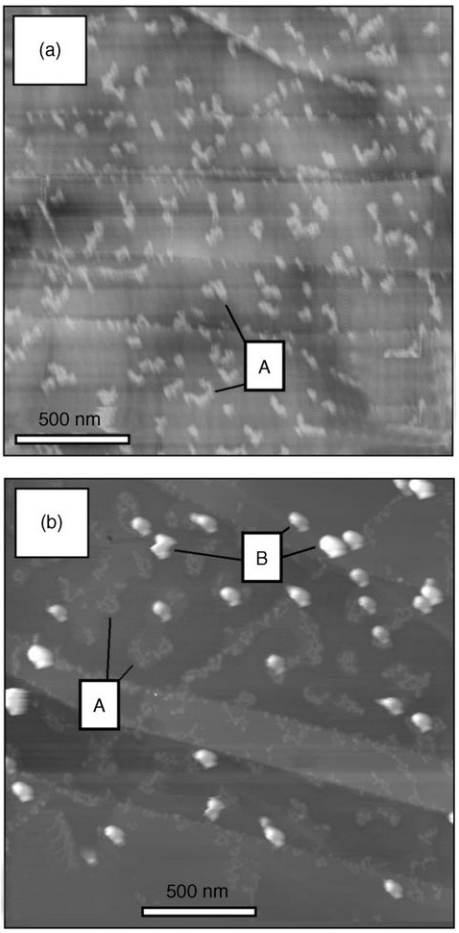

Figure 7. a) AFM topography of an HOPG surface covered with mass-selected BSA fragments. b) BSA deposited with a kinetic energy of 65 eV per charge on HOPG showing fractal (A) and bulky (B) agglomerations. The deposition took place under vacuum (10^{-6} mbar) at room temperature. The height of the fractal aggregations (A) is only half of the low-energy case (see text).

tures are formed following a diffusion-limited-aggregation growth mode. The building units of the fractal clusters are assigned to whole proteins and fragments for the low- and high-energy deposition cases, respectively. In both cases these units have a random coil conformation.

These deposition experiments demonstrate that tracking the beam current allows the control of the molecular coverage. In particular, extremely diluted sub-monolayer films could be prepared, which are suitable for single-molecule studies. Moreover, successive deposition of different molecules could be used to reproducibly create composite films of predetermined relative abundances.

In the near future this experimental setup will be extended to allow ultrahigh vacuum deposition with in situ connection to a variable-temperature scanning tunneling/atomic force microscope. With this apparatus, fundamental investigations of atomic-scale interactions at surfaces will become possible for a variety of aggregates that range from small inorganic clusters to large biomolecules.

4. Experimental Section

The electrospray process takes place under ambient conditions using a commercial electrospray source connected to the deposition setup, which consists of four differential pumping stages. The assembly, as displayed in Figure 1, contains a high- and a low-pressure ion guide (Q1, Q2) and two electrostatic lenses (L1, L2) to form and control the ion beam. In the deposition chamber, a Faraday cup (D), an orthogonal time-of-flight mass spectrometer and a sample holder (T) are mounted.

The solution containing the molecule and the solvent is injected into the electrospray head from a syringe (S) through a spray needle. The spray process is assisted by a nitrogen flow (AG). Experiments were carried out using positive ions created by a high negative voltage of -3500 to -5000 V applied at the counter electrode (E). A heated nitrogen counter gas stream (CG) flows in the upstream direction. The high negative voltage accelerates the sprayed charged droplets against this hot gas flow, which dries the solvent. Once a droplet reaches the Rayleigh limit, where the electrostatic repulsion of its surface charges exceeds the surface tension, smaller droplets occur by Coulomb explosion[22] or jet formation.[23] Continuous iteration of these processes leads to smaller droplets and finally to the isolated charged molecules that form the ion beam. This beam enters the vacuum system through a capillary (C; diameter 0.7 mm, length 15 cm), driven by the pressure difference between the atmospheric side and the first vacuum stage.

Differential pumping begins with a roots pump at the first chamber (P1: 1 mbar). Turbo molecular pumps create a vacuum in the other three chambers (P2: 0.1 mbar, P3: 10^{-4} mbar, P4: 10^{-6} mbar). One stage is connected to the next by small apertures (2 mm in diameter) through which the ion beam can be guided by focusing. A skimmer (Sk) connects the first to the second pumping stage, where the beam is guided within a radio frequency (rf) quadrupole (Q1, 93 mm length, rod diameter 6 mm, trap radius 2.5 mm). The high pressure of the second vacuum stage (0.1 mbar) leads to collisions of the beam ions with the background gas molecules, resulting in a thermalization of the kinetic energy of the particles. By tuning the rf voltage and frequency,[24] the voltage at the quadrupole extraction aperture (A1), and the chamber pressure, it is possible to adjust the mean beam energy and energy distribution.

In the third pumping stage a second quadrupole (Q2, 150 mm length, rod diameter 6 mm, inner radius 2.5 mm) guides the beam. The quadrupole was used in rf-only mode or in mass-selection mode at a fixed frequency of 2.0 MHz depending on the purpose. If high currents were to be achieved (independent of the precise beam composition), the dc voltage difference between the two rod pairs was chosen to be zero. In this case the conditions on the mass-to-charge-ratio for an ion to be transmitted by the quadrupole are less strict. In contrast, to form a beam where the mass-to-charge-ratio of the ions lies within a well-defined range, the quadrupole was used in mass-selection mode, by applying unequal dc voltages at the rod pairs.

In the mass-selection mode, the mass-to-charge transmission window can be estimated by using the stability conditions derived from the Mathieu differential equations.[25] The mean

mass-to-charge-ratio then is given by $m/q = 1.385 \times 10^7\ V_{RF}/f^2r^2$, where f is the drive frequency of the rf voltage V_{RF}, and r is the trap radius.[26] The width of the transmission window can be tuned through variation of the V_{RF}-to-V_{DC} ratio. Due to the fixed frequency of 2 MHz, mass selection is limited to a lower cutoff value of $\approx$500 Da, while the upper cutoff value can be tuned by the dc voltage through the whole mass-to-charge range.

Alternatively, for zero dc voltage (rf-only mode), the conditions for a particle of a certain mass-to-charge-ratio and energy to pass the quadrupole can be estimated using the adiabatic approximation, which yields the minimum and maximum transmitted mass-to-charge-ratios.[25] The minimum value m_{min} is a function of the quadrupole parameters only. The maximum m_{max} decreases with the particle energy and increases with the charge. In Figure 2, the minimum and maximum transmitted mass-to-charge-ratios in rf-only mode are displayed for a kinetic energy of 10 eV and 1, 10, 40, and 100 elementary charges per particle (characteristic values for our experiments).

Typical ions produced by an electrospray source show mass-to-charge-ratios between 600 and 6000,[27] and due to a size-dependent ionization process carry a higher charge when possessing a higher mass.[28] As a consequence, the transmission window of the quadrupole Q2 in rf-only mode becomes larger for bigger, and therefore stronger, charged ions (see Figure 2). The operation of the second quadrupole in rf-only mode thus provides an ion guide for almost all ions generated by ESI.

On the other hand, the rf-only mode, due to the lower drive amplitudes needed, is more suitable for the preparation of a monoenergetic beam. High ac and dc voltages have to be used if high mass resolution is to be achieved, especially for high mass to-charge-ratios. This has the drawback of a less-defined kinetic energy of the particles due to beam heating in the rf field.[27]

Besides other parameters that cannot be changed during the experiment (rf frequency and quadrupole inner radius), the rf amplitude voltage and the kinetic energy determine which particles have stable trajectories. The rf voltage can be tuned up to 500 V (amplitude) to optimize the transmission current. The voltage difference between aperture A1 and the dc offset voltage on quadrupole Q2 accelerates the particles after the thermalization occurring in the first quadrupole and thus determines the energy of the ions in the second quadrupole. In general this energy is different from the incidence energy of the ions on the target. The latter energy is in fact determined by the potential difference between the aperture A1 and the sample.

After leaving the quadrupole, the electrostatic lens system L1 focuses the beam through another aperture finally into the deposition chamber (10^{-6} mbar). In order to have a high deposition current on the sample, a second electrostatic lens system (L2) is used. A removable Faraday cup (D), which is mounted in the chamber, controls the beam current when tuning the beam properties before each deposition experiment. An orthogonal time-of-flight (TOF) mass spectrometer is mounted within the deposition chamber and can be moved into the beam for mass analysis. A plate parallel to the beam axis is pulsed at a 10 kHz repetition rate at 100 V for 4 µs, deflecting the beam almost orthogonally into the drift tube of the TOF spectrometer. The particles reach the detector with an energy of 3 keV.

HOPG was used as the substrate for the deposition. A clean surface was prepared for each experiment by stripping off the top layers with adhesive tape directly before placing the sample in the chamber. The deposition always took place at room temperature. Afterwards the sample was removed from the vacuum chamber and investigated by an atomic force microscope in tapping mode under ambient conditions.

Acknowledgements

This work was supported by the DFG scientific priority program "Semiconductor and Metal Clusters as Building Blocks for Organized Structures" (SPP 1072). The authors acknowledge M. Panthofer for critically reading this manuscript.

[1] M. Mann, R. C. Hendrickson, A. Pandey, *Annu. Rev. Biochem.* **2001**, *70*, 437.
[2] C. W. Tang, S. A. Van Slyke, *Appl. Phys. Lett.* **1987**, *51*, 931.
[3] S. M. Sze, *Physics of Semiconductor Devices*, Wiley-Interscience, New York, **1981**.
[4] B. Kasemo, *Surf. Sci.* **2002**, *500*, 656.
[5] M. A. Reed, C. Zhou, C. J. Muller, T. P. Burgin, J. M. Tour, *Science* **1997**, *278*, 252.
[6] Y. Cui, Q. Wei, H. Park, C. M. Lieber, *Science* **2001**, *293*, 1289.
[7] J. B. Fenn, M. Mann, C. K. Meng, S. F. Wong, C. M. Whitehouse, *Science* **1989**, *246*, 64.
[8] a) G. Siuzdak, B. Bothner, M. Yeager, C. Brugidou, C. M. Fauquet, K. Hoey, C.-M. Chang, *Chem. Biol.* **1996**, *3*, 45; b) S. D. Fuerstenau, W. H. Benner, J. J. Thomas, C. Brugidou, B. Bothner, G. Siuzdak, *Angew. Chem.* **2001**, *113*, 559; *Angew. Chem. Int. Ed.* **2001**, *40*, 542.
[9] V. N. Morozov, T. Y. Morozova, *Anal. Chem.* **1999**, *71*, 1415.
[10] a) G. Siuzdak, T. Hollenbeck, B. Bothner, *J. Mass Spectrom.* **1999**, *34*, 1087; b) C. J. McNeal, R. D. MacFairlane, E. L. Thurston, *Anal. Chem.* **1979**, *51*, 2036; c) M. Danek, K. F. Jensen, C. B. Murray, M. G. Bawendi, *Appl. Phys. Lett.* **1994**, *65*, 2795.
[11] K. Bromann, C. Felix, H. Brune, W. Harbich, R. Monot, J. Buttet, K. Kern, *Science* **1996**, *274*, 956.
[12] a) Z. Ouyang, Z. Takats, T. A. Blake, B. Gologan, A. J. Guymon, J. M. Wiseman, J. C. Oliver, V. J. Davisson, R. G. Cooks, *Science* **2003**, *301*, 1351; b) B. E. Winger, H.-J. Laue, S. R. Horning, R. K. Julian Jr., S. A. Lammert, D. E. Riederer Jr., R. G. Cooks, *Rev. Sci. Instrum.* **1992**, *63*, 5613; c) R. J. Geiger, M. C. Melnyk, K. L. Busch, M. G. Bartlett, *Int. J. Mass Spectrom.* **1999**, *182/183*, 415.
[13] B. Gologan, Z. Takats, J. Alvarez, J. Wiseman, N. Talaty, Z. Ouyang, R. G. Cooks, *J. Am. Soc. Mass Spectrom.* **2004**, *15*, 1874.
[14] J. Varghese, R. B. Cole, *J. Chromatogr.* **1996**, *639*, 303.
[15] L. Bardotti, P. Jensen, A. Hoareau, M. Treilleux, B. Cabaud, A. Perez, F. Aires, *Surf. Sci.* **1996**, *367*, 276.
[16] A. N. Verentchikov, W. Ens, K. G. Standing, *Anal. Chem.* **1994**, *66*, 126.
[17] O. Mori, T. Imae, *Colloids Surf. B* **1997**, *9*, 31.
[18] a) T. Peters, *All about Albumin: Biochemistry Genetics and Medical Applications*, Academic Press, New York, **1996**; b) A. P. Quist, L. P. Björck, C. T. Reimann, S. O. Oscarsson, B. U. R. Sundqvist, *Surf. Sci.* **1995**, *325*, L406.
[19] U. A. Mirza, B. T. Chait, *Int. J. Mass Spectrom.* **1997**, *162*, 173.
[20] T. A. Witten, L. M. Sander, *Phys. Rev. B* **1983**, *27*, 5686.

[21] a) H. Brune, C. Romainczyk, H. Röder, K. Kern, *Nature* **1994**, *369*, 469; b) R. Q. Hwang, J. Schröder, C. Günther, R. J. Behm, *Phys. Rev. Lett.* **1991**, *67*, 3279; c) F.-J. Meyer zu Heringdorf, M. C. Reuter, R. M. Tromp, *Nature* **2001**, *412*, 517.
[22] Lord Rayleigh, *Philos. Mag.* **1882**, *14*, 184.
[23] D. Duft, T. Achtzehn, R. Müller, B. A. Huber, T. Leisner, *Nature* **2003**, *421*, 128.
[24] C. M. Lock, E. W. Dyer, *Rapid Commun. Mass Spectrom.* **1999**, *13*, 422.
[25] D. Gerlich in *Advances in Chemical Physics Series, State-Selected and State-to-State Ion—Molecule Reaction Dynamics, Part 1: Experiment, Vol. 82, Inhomogeneous RF Fields: A Versatile Tool for the Study of Processes with Slow Ions*, (Eds.: C.-Y. Ng, M. Bear), John Wiley & Sons, New York, **1992**, pp. 10–26, 65–70.
[26] P. H. Dawson in *Quadrupole Mass Spectrometry*, (Ed.: P. H. Dawson), Elsevier, Amsterdam, **1976**, pp. 10–24.
[27] M. T. Bowers, A. G. Marshall, F. W. McLafferty, *J. Phys. Chem.* **1996**, *100*, 12897.
[28] J. F. de La Mora, *Anal. Chim. Acta* **2000**, *406*, 93.

Received: December 1, 2005

